富山大学水素同位体科学研究センター研究報告29・30：17－35，2010.

Adsorption/Desorption Processes of H_2O and H_2 over $Cr_2O_3(0001)$ studied by *Ab Initio* Calculation for Small Cluster of Cr3O3

Kuniaki Watanabe, Yuji Torikai, Masanori Hara,
Norio Nunomura* and Ralf D. Penzhorn
Hydrogen Isotope Research Center, University of Toyama
* Information Technology Center
Gofuku 3190, Toyama 930-8555, Japan

(Received May 10th, 2010: Accepted November 1st, 2010)

ABSTRACT

Adsorption/desorption processes of water and hydrogen on the $Cr_2O_3(0001)$ surface were studied by *ab initio* calculations with Gaussian 03 for small clusters of Cr3O3.

It was found that water and hydrogen can be adsorbed molecularly with practically no activation energy. Subsequently the adsorbed molecules are dissociated to form (Cr)OH(a) + (O)H(a) from water and (O)H(a) + (O)H(a) from hydrogen. The process of water adsorption can be described as $H_2O(g)$ + Cr3O3 $\rightarrow$ (Cr3O3)$H_2O(a)$ $\rightleftarrows$ (Cr3O3)$H_2O(a)^*$ $\rightarrow$ (Cr)OH(a)-(O)H(a). The process of hydrogen adsorption is $H_2(g)$ + Cr3O3 $\rightarrow$ (Cr3O3)$H_2(a)$ $\rightleftarrows$ (Cr3O3)$H_2(a)^*$ $\rightarrow$ (Cr)H-(O)H(a) $\rightleftarrows$ (Cr)H-(O)H(a)* $\rightarrow$ 2(O)H(a). With respect to water adsorption, the energies of the adsorbed species were calculated to be -103, -94.8 and -164 kJ/mol for the molecularly adsorbed species, the activated complex and the dissociatively adsorbed species, respectively. Regarding hydrogen adsorption, the energies were -24.7, 38.2, -45.1, 48.0 and -111 kJ/mol for $H_2(a)$, $H_2(a)^*$, (Cr)H-(O)H(a), (Cr)H-(O)H(a)* and (O)H-(O)H(a), respectively. The present results indicate that both water and hydrogen can be dissociatively adsorbed on the Cr_2O_3 surface. However, the dissociative adsorption of water takes place much more easily than that of hydrogen.

1. Introduction

The adsorption of water and hydrogen on pristine oxide layers of stainless steels is of great relevance to the development of tritium-handling techniques, especially from the viewpoint of tritium containment, contamination and decontamination. Since the surface of commonly used type SS316 stainless steel is usually covered with an oxide consisting mainly of Cr_2O_3[1, 2], the behavior of water as well as of hydrogen on this Cr_2O_3 surface needs to be understood in detail.

Two types of tritium contamination of stainless steel may be distinguished: tritium solution in the interstitial sites of the metal bulk and tritium trapping in a thin surface layer consisting of Cr_2O_3[3, 4]. Experimentally it has been shown with a tracer technique that the tritium concentration in the near surface layers is considerably higher than that in the bulk[3, 4, 5]. It was also found that while tritium captured in the bulk can be released into gas phase by

heating under vacuum or under an inert gas atmosphere, the removal of tritium immobilized in the subsurface is much more persistent[3, 4]. In spite of these and other extensive studies the detailed mechanisms of trapping by the surface remains unclear. For example, it is not understood why tritium is predominantly released in the elemental form, HT, into the gas phase under evacuation, and predominantly in the form of HTO into an inert gas atmosphere. It has also been found that the release of tritium solved in the bulk can be explained by diffusion models. The tritium release from the sub-surface layer, on the other hand, cannot be described by a simple diffusion mechanism. This is complicated by the concurrence and/or competition of the diffusion in the sub-surface layer and reactions on the surface.

In the previous study[6], as a first step to understand the tritium capture and release by/from the sub-surface layer of stainless steel, *ab initio* calculations were carried out on the adsorption of H_2O on the $Cr_2O_3(0001)$ surface, which was modeled by a Cr4O4 cluster, using the Gaussian 03 package[7]. Several kinds of adsorbed water species were observed. However, there appeared to be no clear correlation between the structures of adsorbed species and their adsorption energy. This was ascribed to the adopted cluster model, which was too small for this kind of inspection. However, according to calculations for periodic cluster models of $Cr_2O_3(0001)$ by OpenMX[8], one of the adsorbed species described in the previous paper has a quite similar structure with that obtained by OpenMX calculation. On the basis of this observation, the adsorption and desorption processes of H_2O on the $Cr_2O_3(0001)$ surface were examined again in the present study using a small cluster of Cr3O3 and the Gaussian 03 package[7]. The adsorption and desorption processes of H_2 were also examined.

2. Modeling of Oxide Surfaces

Chromium oxide, Cr_2O_3, belongs to the tetragonal-hexagonal group, having $R\bar{3}c$ (#167) structure, conventionally called corundum structure. The lattice parameters are $a = 4.9607$ and $c = 13.599$ Å[9]. It is desirable to simplify the system for calculation to save computational time of Gaussian 03. With the aim of finding more adequate model clusters, preliminary calculations on periodic cluster models for $Cr_2O_3(0001)$ surface were carried out by use of OpenMX[8]. It suggested that a small cluster consisting of six atoms (Cr3O3) is more adequate than one of eight atoms (Cr4O4) adopted in a previous report[6].

In the present investigation, therefore, a six atom cluster as shown in **Fig. 1** was taken as a model of the $Cr_2O_3(0001)$ surface. In the figure the larger balls numbered 1, 5 and 6 correspond to Cr atoms and smaller balls numbered 2, 3 and 4 to O atoms. Together they constitute a Cr3O3 cluster. The plane containing O(2), O(3) and O(4) is parallel to the $Cr_2O_3(0001)$. It can be seen in **Fig.1** of the previous paper[6] that this is also a characteristic configuration of the atoms in the (0001) plane of corundum. **Table 1** shows the locations of six atoms of the Cr3O3 clusters in cartesian coordinates, where the x, y and z values are in Å units. This structure was fixed during the structure optimization for adsorption of H_2O and H_2, by

assuming that no surface relaxation took place owing to the adsorption.

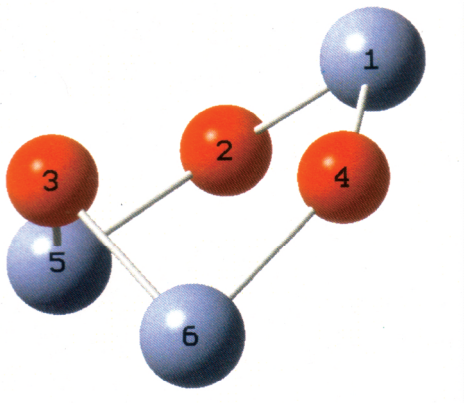

Fig. 1. Structure of the model Cr3O3 cluster

Table 1. Location of the Cr and O atoms in a Cr3O3 cluster in cartesian coordinates

Atom	x	y	z
Cr	1.48978346	-0.85964774	0.90900000
O	2.97929941	0.00000000	0.00000000
O	1.16125153	2.36064290	0.00000000
O	0.00000000	0.00000000	0.00000000
Cr	2.75190803	1.70447152	-0.90900000
Cr	-0.10030949	1.51637528	-1.35700000

3. Structure Optimization

The *ab inito* structural optimization by Gaussian 03 was carried out following the procedures previously described[6]. In the present study, however, some small modifications were made as follows. While the structure of Cr3O3 was fixed as mentioned above, oxygen and hydrogen atoms from H_2O and H_2 molecules were allowed to move freely to find an optimum structure of minimum energy. Geometry optimization was carried out with the model chemistry of "RB3LYP", instead of UB3LYP, and basis functions of Lanl2dz were used for all Cr, O and H atoms. Owing to the rather slow converging speed of calculation by the personal computer used, the optimization started in low convergence criterion with the SCF option of conver=4 and proceeded further with the option of conver=6 [10].

After finding the optimized structure of minimum energy, the total energy of the system was calculated by "RB3LYP" with Lanl2dz for Cr and O atoms, and with 6-31G(d,p) for hydrogen atoms, under the convergence criterion of conver=8. The energy of adsorption was evaluated from the difference in total energy of the system before and after adsorption. For example, the adsorption energy of H_2O is evaluated as

$$E_{ads} = E_{tot}(\text{Cr3O3-H}_2\text{O}) - E_{tot}(\text{Cr3O3} + \text{H}_2\text{O}),$$

where E_{tot}(Cr3O3-H_2O) is the total energy of the system obtained by the structure optimization, E_{tot}(Cr3O3) the total energy of the Cr3O3 cluster, and $E_{tot}(H_2O)$ that of H_2O in the vacuum.

4. Results and Discussion

4.1. Adsorption of H_2O

The calculation showed that H_2O is adsorbed molecularly on a Cr3O3 cluster. It is denoted by $H_2O(a)$-type1 and shown in **Fig.2**. The bond lengths of Cr(1)-O(7), O(7)-H(8) and O(7)-

H(9) were found to be 2.07, 0.97 and 1.02 Å, respectively. The bonding angles of ∠O(7)Cr(1)O(3) and ∠H(8)O(7)H(9) were 86.4 and 112.3°, respectively. The bond length of 2.07 Å is almost equal to the one of $H_2O(a)$-Cr4O4-type-1 (2.00 Å), but a little shorter than 2.18 Å evaluated by OpenMX[11]. The adsorption energy was evaluated to be -103 kJ/mol. This is consistent with the value of -92.6 kJ/mol reported in the previous paper[6] for the species denoted as Cr4O4-type-1. Costa et al. reported a value of -82.6 kJ/mol for molecularly adsorbed water, which was obtained by calculation using the VASP package[12]. According to thermal desorption spectroscopic analysis, the activation energy for the desorption of water, which was formed by exposing the $Cr_2O_3(0001)$ surface to water vapor at 120 K, is 89 kJ/mol[13]. On the other hand, Joly et al.[14] reported that the activation energy for desorption of molecularly adsorbed water was in the range of 110 ∼ 180 kJ/mol for chromium and 304SS. On account of their experimental conditions, it is presumed that the surfaces of their specimens were covered with chromium oxide layers.

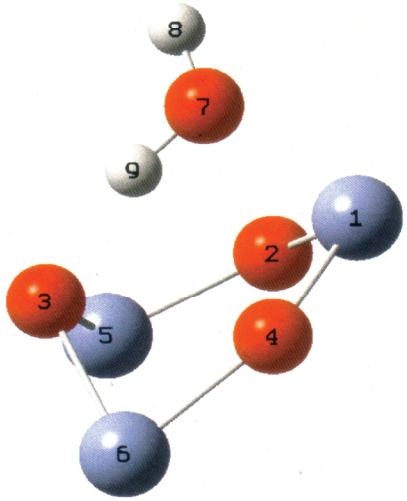

Fig. 2. Molecularly adsorbed $H_2O(a)$ on a Cr3O3 cluster ($H_2O(a)$-type-1)

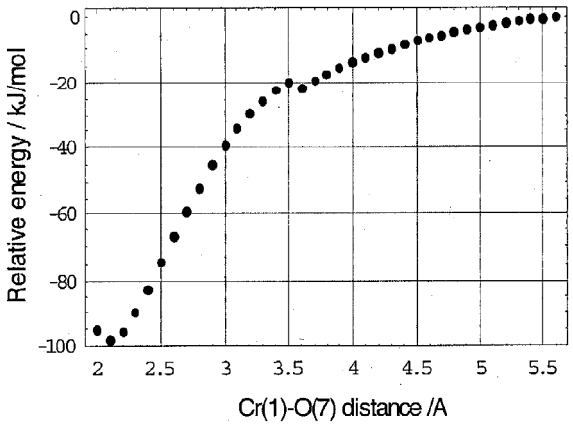

Fig. 3. PES for H_2O approaching Cr(1) (see Fig.2)

Figure 3 shows the result of relaxed potential energy scan (PES) for H_2O approaching Cr(1), where the distance between Cr(1) of the Cr3O3 cluster and O(7) of H_2O molecule were varied in 0.1 Å steps while keeping the angle ∠O(3)Cr(1)O(7) fixed at 90.0° (see Fig.2). Under these conditions, the system geometry was optimized at each step by RB3LYP/Lanl2dz under the SCF convergence criterion of conver=6. The ordinate is the relative energy in kJ/mol, which was defined as the energy change measured from the starting point, and the abscissa is the distance in Å between O(7) and Cr(1). As apparent, the energy of the system monotonically decreases with decreasing distance (the gap about 3.5 Å was due to a small discontinuous change in the H-O-H configuration), the minimum at about 2 Å corresponding to molecular adsorption. This indicates that the molecular adsorption of H_2O can take place without noticeable activation energy. This is the same conclusion as obtained previously for the Cr4O4 cluster.

Figure 4 shows a dissociatively adsorbed H_2O species consisting of Cr(1)-OH and O(3)-H. The bond length of Cr(1)-O(7) was calculated to be 1.79 Å, and those of O(7)-H(8) and O(3)-H(9) to be 0.980 and 0.981 Å, respectively. The energy of the dissociative adsorption was evaluated to be -164 kJ/mol. Basically a similar configuration of the adsorbed species was obtained by OpenMX[11], although there appeared noticeable difference in bonding angles. The ∠O(7)Cr(1)O(3), for example, was 121.3° for the Cr3O3 cluster and 72.8° for the periodic cluster of Cr_2O_3(0001). In particular, the OH group was more slanted towards the (0001) plane of Cr_2O_3 than for the periodic cluster[12]. According to Costa et al., the adsorbed species has a much smaller energy of adsorption about -80 kJ/mol[12] in comparison with the present value. The considerably large difference might be ascribed to the presence of dangling bonds around the corner of Cr3O3 cluster. But it should be mentioned that species like Cr(1)OH-O(3)H might appear at kinks, edges and/or other crystalline planes of Cr_2O_3. In fact, Joly et al. reported a value of 180 ∼ 200 kJ/mol for the activation energy of desorption of dissociatively adsorbed water on chromium or 304L stainless steel[14]. The surfaces of their specimens are considered to be covered with pristine oxide layers consisting of Cr_2O_3.

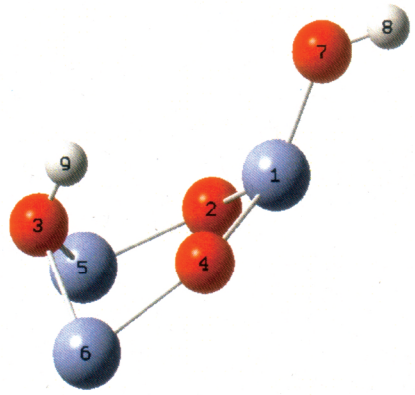

Fig. 4. Dissociative adsorption of H_2O, forming Cr(1)-OH and O(3)-H bonds

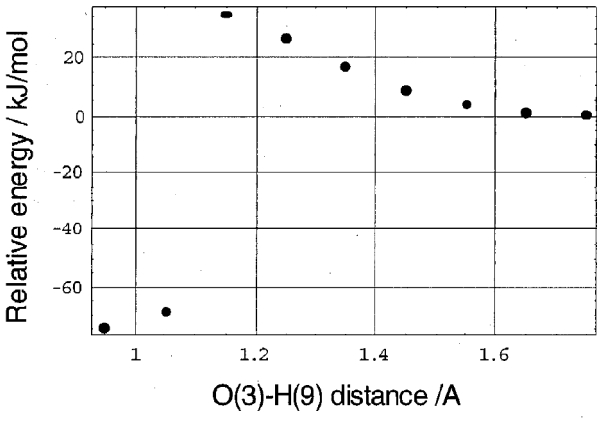

Fig. 5. Relaxed PES for the dissociation of $H_2O(a)$ to form Cr(1)-OH+O(3)-H (see Fig.2)

Figure 5 shows the result of a relaxed PES scan, starting from $H_2O(a)$-type-1, performed to inspect the dissociation to yield Cr(1)-OH + O(3)-H (see Figs.2 and 4). The ordinate gives the relative energy in kJ/mol and the abscissa the distance between O(3) and H(9) in Å. At each motion step in which H(9) comes closer to O(3) by 0.1 Å, a geometry optimization was carried out. It is seen that the energy of the system initially increased with decreasing distance of O(3)-H(9) until 1.15 Å, but after a further approach the energy dropped abruptly with a reconfiguration of atoms to form Cr(1)-OH and O(3)-H bonding. The structure giving the maximum energy was taken as input to find the transition state (TS). The transition state was searched with Opt=TS and/or QST3 keyword of Gaussian-03 by RB3LYP/Lanl2dz under the convergence criterion of conver=6. After finding the transition state structure, the vibration of the system was examined, and if the structure

gave the imaginary frequency corresponding to the motion towards dissociation, the energy of the system was evaluated by Lanl2dz for Cr and O atoms, and 6-31G(d,p) for H atoms for RB3LYP with conver=8 criterion. **Figure 6** is the result of a transition state (TS) search. The bond lengths were 1.97 for Cr(1)-O(7), 1.36 for O(7)-H(9) and 1.18 Å for H(9)-O(3). For this structure, the imaginary frequency towards the dissociation was given as -1465 cm^{-1} and the energy of the system was evaluated to be -94.8 kJ/mol. This means that the activation energy for dissociation to form Cr(1)H-O(3)H from the adsorbed $H_2O(a)$ of type-1 is only 8.2 kJ/mol, agreeing well with the value reported for a periodic cluster model of the $Cr_2O_3(0001)$ surface reported by Costa et al.[12].

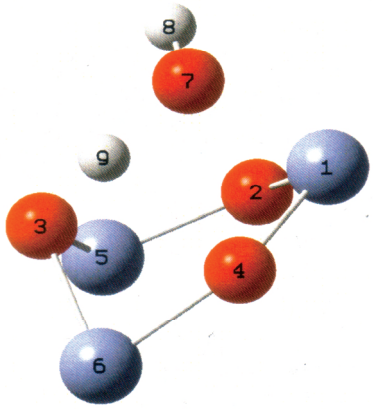

Fig. 6. Transition state structure of Cr(1)OH-HO(3) for dissociation of $H_2O(a)$ to yield Cr(1)OH-O(3)H

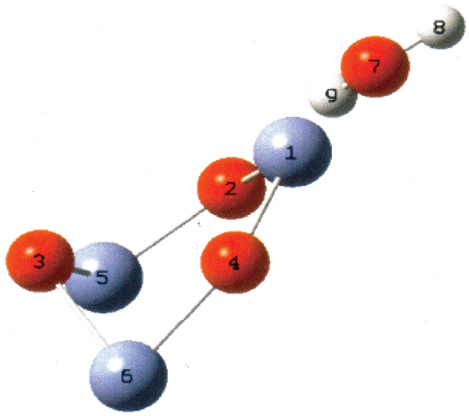

Fig. 7. Molecularly adsorbed $H_2O(a)$ on the Cr3O3 cluster ($H_2O(a)$-type-2)

Figure 7 shows another type of molecularly adsorbed $H_2O(a)$. This configuration will be denoted as $H_2O(a)$-type-2 hereafter. The bond lengths of Cr(1)-O(7) and O(7)-H(8,9) were almost the same as those for type-1, but the dihedral angle between the planes determined by O(4)Cr(1)O(2) and that by Cr(1)O(2)O(7) was found to be 175°. The dihedral angle is denoted by ∠O(4)Cr(1)O(2)O(7) hereafter. The energy of adsorption was evaluated to be -136 kJ/mol.

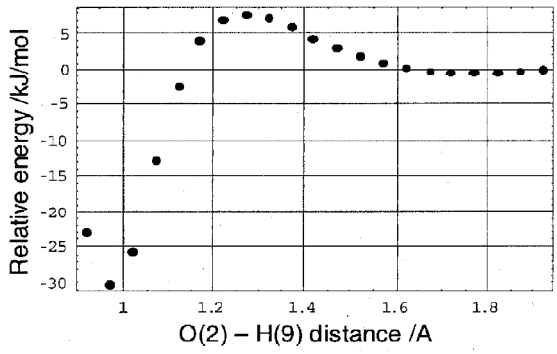

Fig. 8. Relaxed PES for dissociation of $H_2O(a)$ to form Cr(1)-OH+O(2)-H (see Fig.7)

Figure 8 is the result of a relaxed PES scan, where H(9) of $H_2O(a)$ was displaced in 0.1 Å steps towards O(2) of the Cr3O3 cluster (see Fig.7). The ordinate gives the relative energy in kJ/mol and the abscissa the distance between H(9) and O(2) in Å. On the trajectory of H(9) towards O(2), a maximum energy point appears. Upon further approach of H(9) to O(2) dissociation into Cr(1)-OH and O(2)-H takes place. The structure giving the maximum ener-

gy was used as input for the search of transition state towards dissociation.

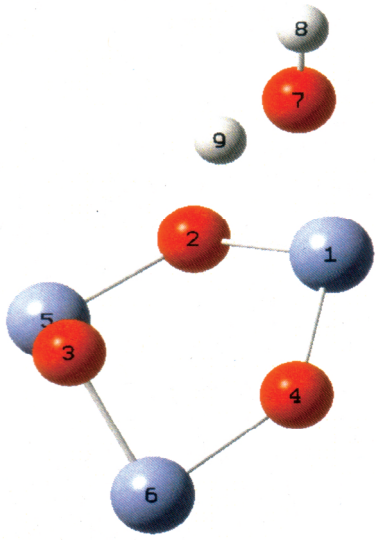

Fig. 9. Transition state from $H_2O(a)$-type-2 to Cr(1)-OH + O(2)-H

Figure 9 shows the activated complex found with the Gaussian 03 keyword of Opt=TS. The obtained bond lengths for Cr(1)-O(7) and O(7)-H(8) were 1.67 and 0.97 Å, respectively. They did not change much from the values for $H_2O(a)$-type-2. The bond length between O(7) and H(9), on the other hand, was appreciably elongated to 1.18 Å. The dihedral angle ∠O(4)Cr(1)O(2)O(7) was 153.1°. The energy of the system was evaluated to be -128 kJ/mol. The energy of Cr3O3-(Cr1)OH-(O2)H was given to be -166 kJ/mol.

The adsorbed species of $H_2O(a)$-type-2, the corresponding activated complex and (Cr1)H-(O2)H species, however, may not be plausible on the (0001) surface of Cr_2O_3, because the bonds of O(2)-H(9) and Cr(1)-O(7) are slanted too much to the (0001) plane. As shown below, this point was inspected by adopting another type of Cr3O3 cluster to account for the effect of nearest neighbor atoms of Cr(1) and O(2) shown in **Fig.7**. The new one is denoted as the O2CrOCr2 cluster. The configuration can be seen in **Fig.10** and the locations of atoms are given in **Table 2**. Cr(1), O(2) and O(3) belong to a given unit cell, and Cr(4), O(5) and O(6) to an adjacent unit cell. The plane determined by O(2), O(3) and O(4) is parallel to the (0001) surface of Cr_2O_3. **Figure 10** shows the molecularly adsorbed $H_2O(a)$ found for the O2CrOCr2 cluster. The bond lengths of Cr(1)-O(7), O(7)-H(8) and O(7)-H(9) were 2.02, 0.97 and 0.98 Å, respectively. The bonding angles of ∠O(7)Cr(1)O(4) and ∠H(8)O(7)H(9) were 82.05 and 115.7°, respectively. The energy of adsorption was evaluated to be -126 kJ/mol.

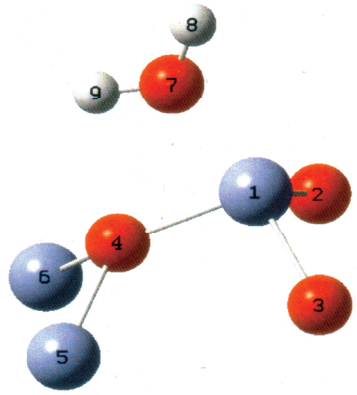

Fig. 10. Moleclulary adsorbed $H_2O(a)$ on a O2CrOCr2 cluster

Table 2. Location of the Cr and O atoms in a O2CrOCr2 cluster in cartesian coordinates

Atom	x	y	z
Cr	0.00000000	0.00000000	0.00000000
O	1.94582009	0.00000000	0.00000000
O	-0.33561230	1.91658142	0.00000000
O	-0.33543578	-0.39930865	1.87464080
Cr	-1.41802479	0.78485882	2.97538891
Cr	0.89145659	-0.90068338	3.42109759

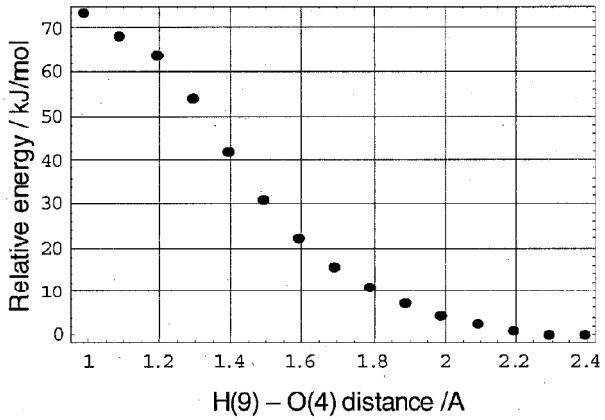

Fig. 11. Relaxed PES for $H_2O(a)$ to form O2CrOCr2-Cr(1)OH-O(4)H (see Fig.10)

Figure 11 shows the result of a relaxed PES scan for O2CrOCr2-$H_2O(a)$ to dissociate into Cr(1)OH-O(4)H, where H(9) of $H_2O(a)$ moved closer to O(4) (see Fig.10). The abscissa represents the relative energy in kJ/mol and the ordinate the distance between O(4) and H(9) in Å. It is seen that the energy increases with decreasing distance, indicating that the dissociation to form Cr(1)OH-O(4)H is energetically unfavorable. This is in accordance with OpenMX calculations, indicating that the dissociation to yield Cr(1)OH-O(4)H type is not likely to take place on the periodic cluster model of Cr_2O_3 (0001) surface.

In conclusion, the dissociative adsorption leading to Cr(1)OH-O(3) can proceed via a molecularly adsorbed state ($H_2O(a)$-type-1) through the transition state shown in **Fig. 6**, where the activation energy for the dissociation of $H_2O(a)$-type-1 is only about 8 kJ/mol.

4.2. Adsorption of H_2

The adsorption process of H_2 was also calculated for Cr3O3 as well as for O2CrOCr2 clusters. **Figure 12** shows the molecularly adsorbed species, $H_2(a)$, found for the Cr3O3 cluster. The bond lengths of H(7)-Cr(1), H(8)-Cr(1) and H(7)-H(8) were 1.83, 1.84 and 0.80 Å, respectively. The dihedral angle of ∠O(3)Cr(1)H(8)H(7) was only 8°, indicating that these atoms are located almost on the same plane. The evaluated energy of adsorption was -24.7 kJ/mol. A relaxed PES scan for the approach of H_2 to Cr(1) resulted in the similar pattern as that shown in **Fig. 3**, indicating that the molecular adsorption of hydrogen is also a non-activated process.

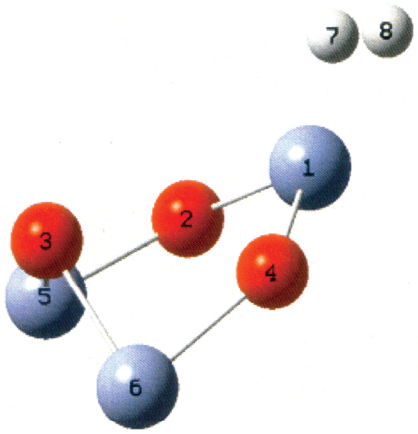

Fig. 12. Moleculary adsorbed $H_2(a)$ on the Cr3O3 cluster

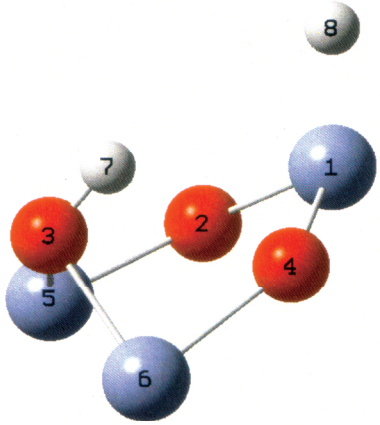

Fig. 13. Dissociative adsorption of H_2, forming Cr(1)-H and O(3)-H bonds

Dissociatively adsorbed H_2 is shown in **Fig. 13**, where H atoms bind to Cr(1) and O(3). The bond lengths of Cr(1)-H and O(3)-H were found to be 1.63 and 0.977, respectively, and the bond angles ∠Cr(1)O(3)H(8) and ∠O(3)Cr(1)H(7) were given to be 58.7 and 110.4°, respectively. The energy of adsorption of this type was evaluated to be -45.1 kJ/mol. To find the reaction path of the dissociation of $H_2(a)$, namely the transition from the state shown in **Fig. 12** to the one shown in **Fig. 13**, a relaxed PES scan was carried out. **Figure 14** presents the result of the calculation, where H(7) was moved in the O(3) direction in steps of 0.1 Å (see Fig.12). It is seen that the energy gradually increases with decreasing distance between H(7) and O(3) and reaches a maximum about 1.3 Å. Further approach of H(7) to O(3) causes a sudden change in the structure, resulting in the dissociation into Cr(1)H-O(3)H.

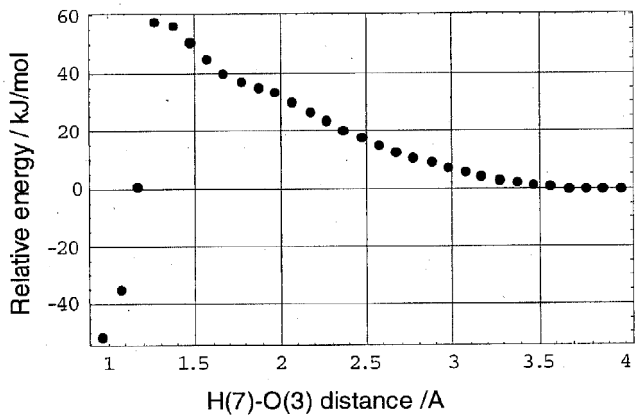

Fig. 14. Relaxed PES for H(7) approachig O(3) (see Fig.12)

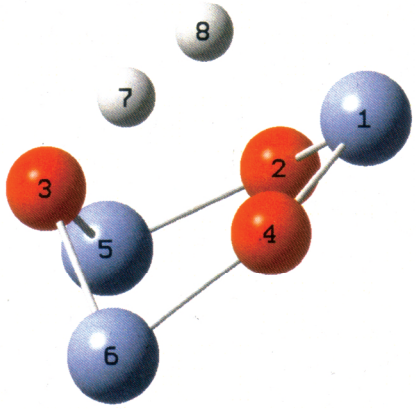

Fig. 15. Activated complex to form Cr(1)H-O(3)H from $H_2(a)$

The structure at the maximum point was subjected to further calculation to shed more light on the transition state. **Figure 15** presents the result of a TS search with Opt=TS by RB3LYP/Lanld2dz and conver=6 options. It is seen that the H(7)-H(8) distance has elongated; its length was calculated to be 1.03 Å. The distance of H(8)-Cr(1) was found to be 1.92 Å and that of H(7)-O(3) 1.24 Å. The bond angles of ∠Cr(1)O(3)H(7) and ∠O(3)Cr(1)H(8) changed to 37.6 and 40.2°, respectively. The dihedral angle of ∠H(7)O(3)Cr(1)H(8) was only 3.8°, indicating that these four atoms are located on almost the same plane. The imaginary vibrational frequency was found to be -1254.5 cm^{-1} and the displacement vector directed rightly toward Cr(1) and O(3). This is considered to be the activated complex connecting $H_2(a)$ and Cr(1)H-O(3)H. The energy of this state was evaluated to be 38.2 kJ/mol. Then the activation energy for the formation of Cr1H-O3H from the molecularly adsorbed $H_2(a)$ is 62.9 kJ/mol.

There appeared in the Cr3O3-H_2 system more stable species such as for instance Cr3O3-O(3)H-O(4)H. This species is shown in **Fig. 16**. The bond lengths of H(7)-O(4) and H(8)-O(3) were found to be 0.986 and 0.985 Å, respectively. The bond angles of ∠H(8)O(3)O(4) and

∠H(7)O(4)O(2) were 73.8 and 154.1°, respectively. This indicates that the H(8)-O(3) bond is nearly normal. On the other hand, the H(7)-O(4) bond is almost parallel to the Cr_2O_3 (0001) plane, which means that the bond is headed to the O atom in the adjacent unit cell. The energy of this system was evaluated to be -111 kJ/mol. This species could not be formed directly from $H_2(a)$. One possible route of formation is hydrogen transfer from Cr(1)H to O(4)H. **Figure 17** shows the transition state for this transformation. The bond length of H(8)-O(3) was 0.998 Å and the angle ∠H(8)O(3)O(4) 65.4°. The bond lengths of Cr(1)-H(7) and O(4)-H(7) were 1.77 and O(4)-H(7) 1.49 Å, respectively. The dihedral angle of ∠O(3)O(4)O(2)H(7) was 72.4°, indicating that H(7) is almost normal to the (0001) plane of Cr_2O_3. The imaginary frequency was -1311 cm^{-1} and the displacement vector was directed rightly toward O(4). The energy evaluated gave 48.0 kJ/mol. The activation energy for the transformation from Cr(1)H to O(4)H was calculated to be 93.1 kJ/mol.

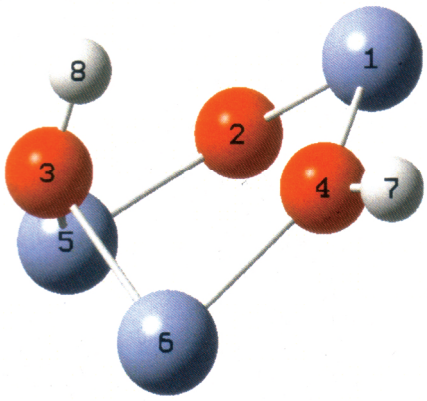

Fig. 16. Adsorbed species of O(3)H-O(4)H

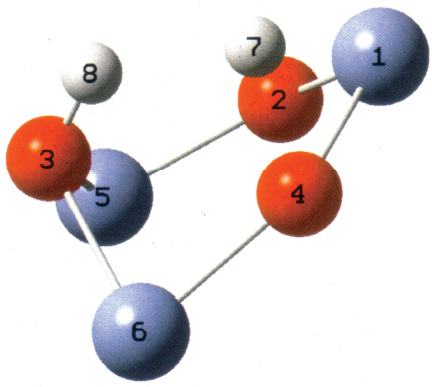

Fig. 17. Activated complex to form O(3)H-O(4)H from Cr(1)H-O(3)H

In conclusion, dissociative adsorption of H_2 can take place via molecularly adsorbed $H_2(a)$ through a transition state such as shown in **Fig. 15** to yield Cr(1)H and O(3)H. The activation energy for the dissociation of $H_2(a)$ was calculated to be 62.9 kJ/mol. This species can further transform to the O(3)H-O(4)H state via the transition state depicted in **Fig. 17**, the activation energy for the transformation being about 93 kJ/mol.

Table 3. Adsorbed species, energy and atomic configuration of the Cr3O3-H_2O and -H_2 systems in Z-matrix form

species/energy	atom	atom	length[a)]	atom	angle[b)]	atom	dihedral[b)]
Cr3O3-$H_2O(a)$(type-1)	H(8)	O(7)	0.973	Cr(5)	131.1	O(3)	-123.7
-103 kJ/mol	H(9)	O(7)	1.02	Cr(5)	97.4	O(3)	5.53
	H(9)	O(3)	1.75	Cr(5)	43.7	O(7)	-4.62
Cr3O3-$H_2O(a)^*$	H(8)	O(7)	0.981	Cr(5)	115.8	O(3)	-108.1
TS	H(9)	O(7)	1.364	Cr(5)	100.0	O(3)	6.26
-94.8 kJ/mol	H(9)	O(3)	1.18	Cr(5)	40.3	O(7)	-11.1

(Continued)

species/energy	atom	atom	length[a)]	atom	angle[b)]	atom	dihedral[b)]
Cr1OH-O3H	H(8)	O(7)	0.980	Cr(1)	129.7	O(3)	-174.4
-164 kJ/mol	H(9)	O(3)	0.981	Cr(1)	57.8	O(7)	-15.9
Cr3O3-$H_2(a)$	H(8)	Cr(1)	1.84	O(3)	120.2	H(7)	-3.51
-24.7 kJ/mol	H(7)	H(8)	0.80	Cr(1)	76.4	O(3)	8.22
Cr3O3-$H_2(a)^*$	H(8)	Cr(1)	1.92	O(3)	40.2	H(7)	-3.80
TS	H(7)	O(3)	1.24	Cr(1)	37.6	H(8)	-3.80
38.2 kJ/mol	H(7)	H(8)	1.03				
Cr1H-O3H	H(7)	Cr(1)	1.63	O(3)	110.4	H(8)	-21.2
-45.1 kJ/mol	H(8)	O(3)	0.977	Cr(1)	58.7	H(7)	-21.2
Cr1H-O4H	H(7)	O(4)	1.49	O(3)	68.0	H(8)	-3.2
TS	H(8)	O(3)	0.998	Cr(1)	52.5	O(4)	100.1
48.0 kJ/mol	H(8)	H(7)	1.73				
O3H-O4H	H(7)	O(4)	0.986	O(3)	140.3	H(8)	76.0
-111 kJ/mol	H(8)	O(3)	0.985	Cr(1)	62.0	O(4)	101.9

a) length in Å; *b*) angle in degree

Table 3 summarizes the energies of adsorption for both water and hydrogen along with the geometric parameters of adsorbed species.

4.3. Kinetic evaluation

The *ab initio* calculations by Gaussian 03 indicated that the adsorption and desorption of water on the surface of Cr_2O_3 (0001) most likely proceeds according to

$$H_2O(g) + Cr3O3 \underset{\overleftarrow{k_1}}{\overset{\overrightarrow{k_1}}{\rightleftharpoons}} (Cr3O3)\text{-}H_2O(a) \quad \text{(type-1)} \tag{1}$$

$$(Cr3O3)\text{-}H_2O(a) \quad \text{(type-1)} \rightleftarrows (Cr3O3)\text{-}H_2O(a)^* \xrightarrow{\overrightarrow{k_2}} (Cr)OH\text{-}(O)H(a) \tag{2}$$

$$(Cr3O3)\text{-}H_2O(a) \quad \text{(type-1)} \xleftarrow{\overleftarrow{k_2}} (Cr3O3)\text{-}H_2O(a)^* \rightleftarrows (Cr)OH\text{-}(O)H(a) \tag{2'}$$

As for hydrogen, the processes can be written as

$$H_2(g) + Cr3O3 \underset{\overleftarrow{k_3}}{\overset{\overrightarrow{k_3}}{\rightleftharpoons}} (Cr3O3)\text{-}H_2(a) \tag{3}$$

$$(Cr3O3)\text{-}H_2(a) \rightleftarrows (Cr3O3)\text{-}H_2(a)^* \xrightarrow{\overrightarrow{k_4}} (Cr)H\text{-}(O)H(a) \tag{4}$$

$$(Cr3O3)\text{-}H_2(a) \xleftarrow{\overleftarrow{k_4}} (Cr3O3)\text{-}H_2(a)^* \rightleftarrows (Cr)H\text{-}(O)H(a) \tag{4'}$$

$$(Cr)H\text{-}(O)H(a) \rightleftarrows (Cr)H\text{-}(O)H(a)^* \xrightarrow{\overrightarrow{k_5}} (O)H\text{-}(O)H(a) \tag{5}$$

$$(Cr)H\text{-}(O)H(a) \xleftarrow{\overleftarrow{k_5}} (Cr)H\text{-}(O)H(a)^* \rightleftarrows (O)H\text{-}(O)H(a) \tag{5'}$$

Some of the stable species showed vibrational modes with imaginary frequencies, which made it difficult to evaluate correctly the vibrational partition functions, the pre-exponential

factors and zero-point energies. The imaginary frequencies are largely due to the adoption of a rigid Cr3O3 cluster model, which induces new coupling with the adsorbed species, giving rise to complex vibrational modes coupled with the newly formed (Cr)-OH and (O)-H bonds. Nevertheless it should be worthwhile to discuss here the reaction rates as a semi-quantitative guideline. In the following sections, adsorption/desorption kinetics of water and hydrogen are discussed according to the evaluated energies of adsorption along with the results of vibration analyses. The potential energy diagrams for adsorption of water and of hydrogen are given in **Figs. 18 and 19**, respectively, for reader' s convenience.

4.3.1. Adsorption and Desorption of Water

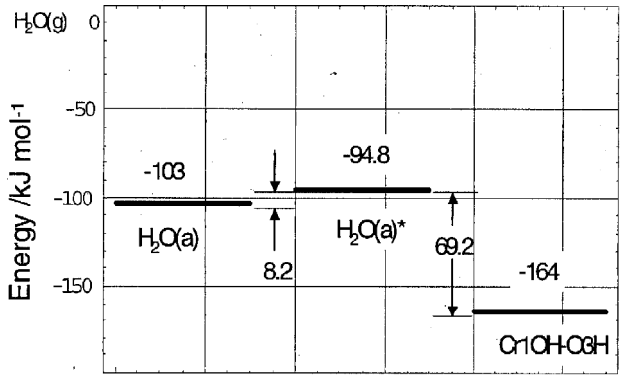

Fig. 18. Energy diagram of H_2O adsorption for Cr3O3 cluster

The first step of water adsorption was found to be non-activated. In this case, the supposed activated complex can be treated like a two dimensional gas[15], for which the adsorption rate is simply given by the Knudsen equation

$$\overrightarrow{v_1} = p_{H_2O}/\sqrt{2\,\pi\, m_{H_2O}\, k_B\, T} \quad \mathrm{cm^{-2}\cdot s^{-1}} \quad (6)$$

This is also true for the first step of hydrogen adsorption. In this case, p_{H_2O} and m_{H_2O} in the above equation should be replaced by p_{H_2} and m_{H_2}, respectively.

The rate of the second step reaction, eq.(2), can be described as

$$\overrightarrow{v_2} = \overrightarrow{k_2}\,[H_2O(a)] = [H_2O(a)] \left(\frac{k_B\,T}{h}\right) \left(\frac{Q^*_{\mathrm{H_2O}(a)}}{Q_{H_2O(a)}}\right) \exp(-\Delta E/k_B T), \quad (7)$$

where the concentration of the species in brackets will be measured in "molecules $\mathrm{cm^{-2}}$ " ; $Q^*_{\mathrm{H_2O}(a)}$ and $Q_{H_2O(a)}$ are the total partition functions of the activated complex and the adsorbed H_2O molecule, respectively. They are given by the surface saturation density N_s ($\mathrm{cm^{-2}}$) times the complete partition functions for the adsorbed species themselves[16]. In this case, (Cr3O3)-$H_2O(a)^*$ should be localized and its rotational motion be hampered. (Cr3O3)-$H_2O(a)$ appeared to be also localized but the rotational motion could take place. The rate constant in eq.(7) is expressed as

$$\overrightarrow{k_2} = \left(\frac{k_B\,T}{h}\right) \left(\frac{q^*_{v_{\mathrm{H_2O}(a)}}}{q_{v_{H_2O(a)}}\; q_{r_{H_2O(a)}}}\right) \exp(-\Delta E/k_B T), \quad (8)$$

where q_v and q_r denote the vibrational and rotational partition functions, respectively; the translation partition functions for localized adsorbed species and for hampered rotation are taken to be unity[15]. Accordingly, there appears only the vibrational partition function for the activated complex. The rotational partition function for the rotation of H around Cr-O of

$H_2O(a)$ axis was calculated to be about 3[17]. The ratio of vibrational partition function of (Cr)OH-(O)H* to the reactants was about 1 at 300 K. The rate constant then becomes

$$\overrightarrow{k_2} = 2.07 \times 10^{12} \exp(-8.2 \times 10^3/RT) \ \mathrm{s}^{-1}, \tag{8'}$$

where the activation energy in J/mol is evaluated from the difference between the classical energies for Cr3O3-$H_2(a)$* and Cr3O3-$H_2(a)$ (see **Table 3 and Fig.18**).

The rate of the reverse reaction of eq.(1) is simply given by

$$\overleftarrow{v_1} = \overleftarrow{k_1}\,[H_2O(a)] \tag{9}$$

$$\begin{aligned}\overleftarrow{k_1} &= \left(\frac{k_B\,T}{h}\right) \exp(-\Delta E/k_B\,T) \\ &= 6.25 \times 10^{12} \exp(-103 \times 10^3/R\,T) \ \mathrm{s}^{-1},\end{aligned} \tag{10}$$

Concerning the back reaction, eq.(2'), the reaction rate is

$$\overleftarrow{v_2} = \overleftarrow{k_2}\,[(Cr)OH(a)][(O)H(a)] \tag{11}$$

$$\begin{aligned}\overleftarrow{k_2} &= \left(\frac{1}{N_s}\right)\left(\frac{k_B\,T}{h}\right)\left(\frac{q^*_{v_{H_2O(a)}}}{q_{v(Cr)OH(a)}\,q_{r(Cr)OH(a)}\,q_{v(O)H(a)}}\right) \\ &\quad \times \exp(-\Delta E/k_BT) \ \mathrm{cm}^2\cdot\mathrm{s}^{-1},\end{aligned} \tag{12}$$

where N_s was set to 1×10^{15} cm^{-2}, and the rotational partition function of (Cr)OH for the rotation of H around Cr-O axis was about 2 at 300 K. The ratio of vibrational partition function between (Cr)OH-(O)H*(a) and reactants were taken to be 0.87. Accordingly the numerical values for the rate constant is

$$\overleftarrow{k_2} = 2.72 \times 10^{-3} \exp(-69.2 \times 10^3/RT) \ \mathrm{cm}^2\cdot\mathrm{s}^{-1} \tag{12'}$$

4.3.2. Adsorption and Desorption of Hydrogen

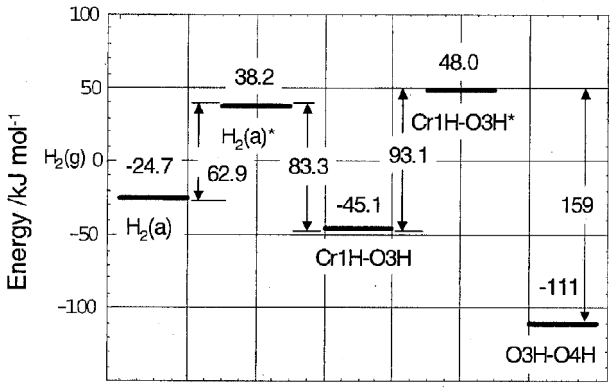

Fig. 19. Energy diagram of H_2 adsorption for Cr3O3 cluster

With respect to the adsorption of hydrogen, the rate of the first step is given by a similar equation as eq.(6), where p_{H_2O} and m_{H_2O} should be read as p_{H_2} and m_{H_2}, respectively. The desorption rate of molecularly adsorbed hydrogen is given by

$$\overleftarrow{v_3} = \overleftarrow{k_3}\,[H_2(a)] \tag{13}$$

$$\begin{aligned}\overleftarrow{k_3} &= \left(\frac{k_B\,T}{h}\right) \exp(-\Delta E/k_BT) \\ &= 6.25 \times 10^{12} \\ &\quad \times \exp(-24.7 \times 10^3/k_BT) \ \mathrm{s}^{-1}\end{aligned} \tag{14}$$

Concerning the second step, eq.(4), the adsorbed $H_2(a)$ is considered to be localized, the reaction rate becoming

$$\overrightarrow{v_4} = \overrightarrow{k_4}[H_2(a)] \tag{15}$$

$$\overrightarrow{k_4} = \left(\frac{k_B T}{h}\right)\left(\frac{q^*_{v_{H_2(a)}}}{q_{v_{H_2(a)}}\, q_{r_{H_2(a)}}}\right)\exp(-\Delta E/k_B T),$$

$$= 6.25 \times 10^{12}\exp(-62.9 \times 10^3/RT)\ \mathrm{s}^{-1}, \tag{16}$$

where the numerical values at 300 K were taken as 1 for the rotational partition function of $H_2O(a)$ and about 1 for the ratio of the vibrational partition function of $H_2O(a)^*$ to that of $H_2O(a)$. Those for the activation enery can be seen in **Fig.19** and **Table 3**.

The reaction rate for the third step, eq.(5), is

$$\overrightarrow{v_5} = \overrightarrow{k_5}\,[(Cr)H(a)][(O)H(a)] \tag{17}$$

$$\overrightarrow{k_5} = (\frac{1}{N_s})\left(\frac{k_B T}{h}\right)\left(\frac{q^*_{v_{(Cr)H\text{-}(O)H(a)}}}{q_{v_{(Cr)H(a)}}\, q_{v_{(O)H(a)}}}\right)\exp(-\Delta E/k_B T)$$

$$= 6.25 \times 10^{-3}\exp(-93.1 \times 10^3/RT)\ \mathrm{cm^2{\cdot}s^{-1}}, \tag{18}$$

where it was taken into account that the ratio of the vibrational partition function of the activated complex to those of the adsorbed species was about 1 at 300 K.

Concerning the reverse reaction, eq.(5'), the reaction rate is

$$\overleftarrow{v_5} = \overleftarrow{k_5}\,[(O)H(a)]^2 \tag{19}$$

$$\overleftarrow{k_5} = (\frac{1}{N_s})\left(\frac{k_B T}{h}\right)\left(\frac{q^*_{v_{(CrO)H(a)}}}{q^2{}_{v_{(O)H(a)}}}\right)\exp(-\Delta E/k_B T),$$

$$= 5.63 \times 10^{-3}\exp(-159 \times 10^3/RT)\ \mathrm{cm^2{\cdot}s^{-1}}, \tag{20}$$

since the ratio of the partition function was evaluated to be 0.90.

The rate of backward reaction of eq.(4') is

$$\overleftarrow{v_4} = \overleftarrow{k_4}\,[(Cr)H(a)][(O)H(a)]\ \mathrm{cm^{-2}{\cdot}s^{-1}}, \tag{21}$$

$$\overleftarrow{k_4} = (\frac{1}{N_s})\left(\frac{k_B T}{h}\right)\left(\frac{q^*_{v_{H_2}(a)}}{q_{v_{(Cr)H(a)}}\, q_{v_{(O)H(a)}}}\right) \times \exp(-\Delta E/k_B T),$$

$$= 6.25 \times 10^{-3}\exp(-83.3 \times 10^3/RT)\ \mathrm{cm^2{\cdot}s^{-1}} \tag{22}$$

4.3.3. Thermal Desorption Spectra

It is interesting to compare calculated thermal desorption spectra of water with observed ones. **Figure 20** shows the thermal desorption spectra calculated for molecularly adsorbed water. Spectrum (a) was obtained with E_d = 89 kJ/mol reported by Henderson et al.[13] and a frequency factor of 1.0×10^{13} s^{-1} for the initial coverage of 1×10^{15} cm^{-2} with a temperature ramp of 2 K s^{-1}. This spectrum agrees quite well with the experimental one[6, 13]. On the

other hand, calculation by applying $E_d = 103$ kJ/mol and the frequency factor of 6.25×10^{12} s^{-1} gave the spectrum (b). The peak temperature is about 50 K higher than that of the spectrum (a). Although exact fit could be achieved by taking the frequency factor of 1×10^{15} s^{-1}, this value is considerably larger than that expected for this case of around 1×10^{13} s^{-1}. It means that the value of 103 kJ/mol appears to be over estimated by at least 5 kJ/mol.

With respect to the desorption of dissociatively adsorbed water, since the potential barrier between $H_2O(a)$ and (Cr)OH+(O)H(a) is quite low as seen in **Fig. 18**, they could be considered to be in equilibrium; viz. $\overrightarrow{v_2} = \overleftarrow{v_2}$. Accordingly, the reaction scheme can be written as

$$(\mathrm{Cr})\mathrm{OH}(a) + (\mathrm{O})\mathrm{H}(a) \rightleftharpoons \mathrm{H_2O}(a) \quad (23)$$

$$\mathrm{H_2O}(a) \rightarrow \mathrm{H_2O}(g) \quad (24)$$

and the desorption rate of dissociatively adsorbed water is

$$\overrightarrow{v}_{H_2O(g)} = [(Cr)OH(a)]\,[(O)H(a)](\frac{k_B T}{h})(\frac{\overleftarrow{k_2}}{\overrightarrow{k_2}})\exp(-103 \times 10^3/RT) \quad (25)$$

$$= 8.21 \times 10^{-3}\exp(-164 \times 10^3/RT)[(Cr)OH(a)][(O)H(a)]\ \mathrm{cm^{-2}\cdot s^{-1}} \quad (26)$$

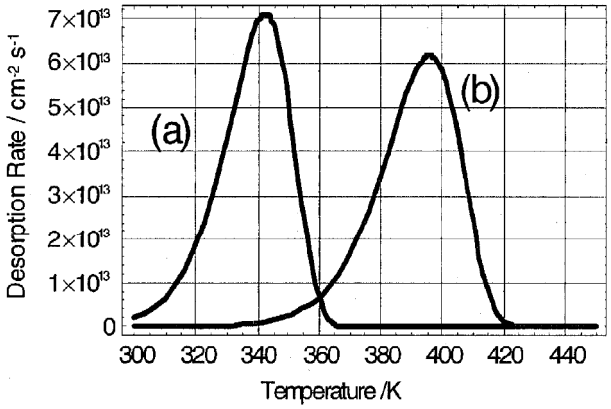

Fig. 20. Calculated thermal desorption spectra for molecularly adsorbed water; using (a) E_d = 89 kJ/mol and $\nu = 1 \times 10^{13}$ s^{-1}, or (b) E_d = 103 kJ/mol and $\nu = 6.25 \times 10^{12}$ s^{-1}, at 2 K s^{-1}

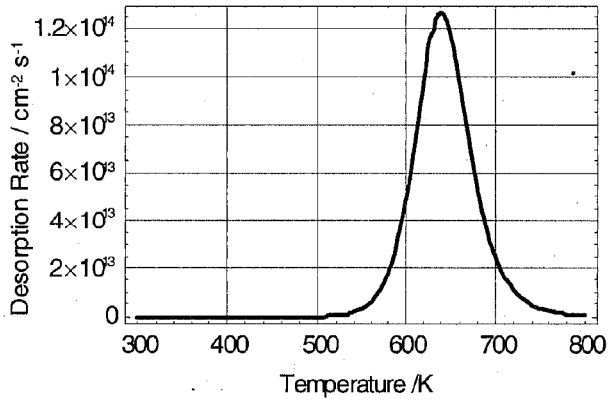

Fig. 21. Calculated thermal desorption spectrum for dissociatively adsorbed water; applying the values of E_d = 164 kJ/mol and ν = 8.21×10^{-3} cm^2 s^{-1}, at 10 K s^{-1}

Figure 21 shows a thermal desorption spectrum calculated following eq.(26). For the calculation, an initial coverage of 1×10^{15} cm^{-2} and a temperature ramp of 10 K s^{-1} were adopted. As apparent the spectrum shows a rather sharp peak at about 640 K. The temperature at which the peak reaches maximum value agrees quite well with that observed by Joly et al.[14] for chromium, which is supposed to be covered by pristine oxide layer before exposure to water at 473 K. The only difference was that their peak was much broader. The matching suggests that the dissociatively adsorbed water found in the present study constitutes a substantial part of the water desorbed at the high temperature region in the thermal desorption spectrum.

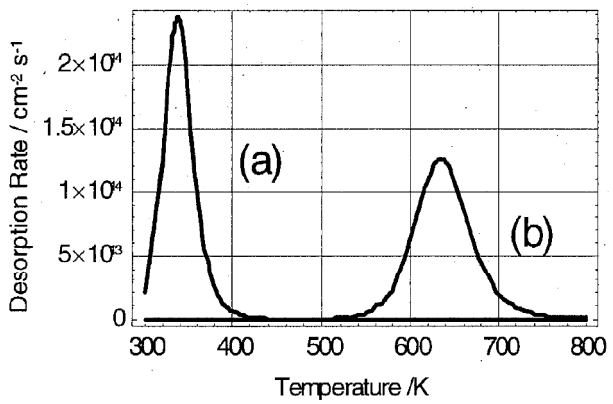

Fig. 22. Calculated theraml desorption spectrum for; (a) (Cr)H-(O)H with the values of E_d = 83.3 kJ/mol and $\nu = 6.25 \times 10^{-3}$ cm^2 s^{-1}; (b) (O)H-(O)H with the values of E_d = 159 kJ/mol and $\nu = 5.68 \times 10^{-3}$ cm^2 s^{-1}, at 10 K s^{-1}

Figure 22 shows calculated desorption spectra of hydrogen from (Cr)H-(O)H(a) and (O)H-(O)H(a). In this case, the desorption rate of molecularly adsorbed hydrogen is very rapid and the process does not play a role in the overall desorption spectrum. In addition, since there is a large difference in the desorption rates described by eqs.(19) and (21), the desorption spectrum for each of the adsorbed states can be calculated separately. Under the conditions that the initial coverage is 1×10^{15} cm^{-2} and the temperature ramp is 10 K s^{-1}, the desorption spectra of hydrogen from (Cr)H-(O)H(a) and (O)H-(O)H(a) were calculated. Spectrum (a) was derived from eqs.(21,22) and the spectrum (b) from eqs.(19,20). It is seen in the figure that desorption peak of the spectrum (a) appears at 320 K, while that of spectrum (b) is observed at a far higher temperature, i.e., 630 K. It is worthwhile to mention that the hydrogen desorption from (Cr)H-(O)H(a) state takes place in almost the same temperature range with that of water desorption from the molecularly adsorbed state. But once the hydrogen atom of (Cr)H-(O)H(a) has moved to the adjacent O-site to transform to (O)H-(O)H(a) state, the hydrogen desorption becomes far slower to take place in the similar temperature range with that of water desorption from the dissociatively adsorbed water.

The above discussed desorption characteristics imply that tritium captured by the (0001) surface of Cr_2O_3 can be removed via molecularly adsorbed THO(a), and also through (Cr)T-(O)H(a) or (Cr)H-(O)T(a) states at low temperature. The adsorbed HTO(a) can be easily formed via the equilibrium reaction of HTO(a) $\rightleftarrows$ (Cr)OH-(O)T(a) or (Cr)OT-(O)H(a) in a wet atmosphere. On the other hand, desorption of HT at low temperature can take place under the conditions that there is initially enough hydrogen atoms on the Cr-sites as (Cr)H(a) or (Cr)T(a), or otherwise enough supply of hydrogen from the environment. In the region of higher temperature, the initially existing (Cr)OH(a) and (Cr)H(a) should be released during temperature raise. The detritiation proceeds via reactions (5') and (4'), releasing HT by the reverse reaction (3) into a dry atmosphere and/or into high vacuum. It is interesting to note that diffusion of tritium captured in the bulk to the surface is enhanced at high temperature and then the tritium captured in the bulk region can be also removed as HT in gas phase by this mechanism, where the existence of (Cr)H(a) or (Cr)T(a) is essential. Hydrogen in the gas phase will further enhance this reaction, because it yields (Cr)H(a) or (Cr)T(a) and these species can play a role as a reaction intermediate for HT release by this mechanism. At high

temperature and a not fully dry atmosphere such as poor vacuum or Ar-gas flow having a poor dew point, there will be enough supply of water to form (Cr)OH(a) although the surface concentration of $H_2O(a)$ should be significantly low. But since the molecularly adsorbed water acts as a reaction intermediate, a trace amount of $H_2O(a)$ is enough to extract tritium captured in the bulk and release it as HTO into the gas phase.

In summary, it was shown that thermal desorption spectra for adsorbed water and hydrogen could be calculated from theoretically obtained numerical rate constants. In spite of the good results, there remains ambiguity about the zero-point energy corrections and the partition functions of adsorbed species. The validity of small rigid cluster models must be examined further by comparing with *ab initio* calculations for periodic clusters with and without surface relaxation. More work on this topic is currently under way.

5. Conclusions

Adsorption/desorption processes of water and hydrogen on Cr_2O_3 surface were studied adopting small cluster as Cr3O3 by *ab initio* calculations using Gaussian 03 package. The cluster was embraced by assuming (0001) surfaces of Cr_2O_3. It was found that molecular and dissociative adsorption could take place with both water and hydrogen, the molecular adsorption preferentially occurring on a Cr atom.

The dissociative adsorption of water takes place through the activated complex, Cr3O3-$H_2O(a)^*$, to yield (Cr)OH-(O)H(a). The reaction describing the process is $H_2O(g) + Cr3O3 \rightarrow$ Cr3O3-$H_2O(a) \rightleftarrows$ Cr3O3-$H_2O(a)^* \rightarrow$ (Cr)OH-(O)H(a). The energies were calculated to be -103, -94.8, -164 kJ/mol for molecular adsorption, activated complex and dissociatively adsorbed water, respectively.

Similarly the dissociative adsorption of hydrogen proceeds via activated complexes such as Cr3O3-$H_2(a)^*$ and (Cr)H-(O)H$(a)^*$ to form (O)H-(O)H(a). The process can be described by the reaction sequence of $H_2(g)$ + Cr3O3 $\rightarrow$ Cr3O3-$H_2(a) \rightleftarrows$ Cr3O3-$H_2(a)^* \rightarrow$ (Cr)H-(O)H$(a) \rightleftarrows$ (Cr)H-(O)H$(a)^* \rightarrow$ (O)H-(O)H(a). The energies were calculated to be -24.7, 38.2, -45.1, 48.0 and -111 kJ/mol for Cr3O3-$H_2(a)$, Cr3O3-$H_2(a)^*$, (Cr)H-(O)H(a), (Cr)H-(O)H$(a)^*$ and (O)H-(O)H(a), respectively.

For both water and hydrogen adsorption/desorption, the forward and backward reaction rates were estimated and thermal desorption spectra clarified characteristic features of their desorption.

References

[1] Y. Hatano, T. Maetani and M. Sugisaki, *Fusion Technol.*, 28 (1995) 1182

[2] J. E. Castle and C. R. Clayton, *Corrosion Sci.*, 17 (1997) 7

[3] Y. Torikai, R-D. Penzhorn, M. Matsuyama and K. Watanabe, *Fusion Sci. Technol.*, 48 (2005) 177

[4] Y. Torikai, M. Murata, R-D. Penzhorn, K. Akaishi, K. Watanabe and M. Matsuyama, *J. Nucl. Mater.*, 363-365 (2007) 462

[5] R-D. Penzhorn, Y. Torikai, M. Matsuyama and K. Watanabe, *J. Nucl. Mater.*, 353 (2006) 66

[6] K. Watanabe, M. Hara, Y. Torikai and Y. Hatano, *Ann. Rept. Hydrogen Isot. Res. Centr.*, 28 (2008) 9

[7] M. J. Frisch, G. W. Trucks, H. B. Schlegel, G. E. Scuseria, M. A. Robb, J. R. Cheeseman, Jr. J. A. Montgomery, T. Vreven, K. N. Kudin, J. C. Burant, J. M. Millam, S. S. Iyengar, J. Tomasi, V. Barone, B. Mennucci, M. Cossi, G. Scalmani, N. Rega, G. A. Petersson, H. Nakatsuji, M. Hada, M. Ehara, K. Toyota, R. Fukuda, J. Hasegawa, M. Ishida, T. Nakajima, Y. Honda, O. Kitao, H. Nakai, M. Klene, X. Li, J. E. Knox, H. P. Hratchian, J. B. Cross, C. Adamo, J. Jaramillo, R. Gomperts, R. E. Stratmann, O. Yazyev, A. J. Austin, R. Cammi, C. Pomelli, J. W. Ochterski, P. Y. Ayala, K. Morokuma, G. A. Voth, P. Salvador, J. J. Dannenberg, V. G. Zakrzewski, S. Dapprich, A. D. Daniels, M. C. Strain, O. Farkas, D. K. Malick, A. D. Rabuck, K. Raghavachari, J. B. Foresman, J. V. Ortiz, Q. Cui, A. G. Baboul, S. Clifford, J. Cioslowski, B. B. Stefanov, G. Liu, A. Liashenko, P. Piskorz, I. Komaromi, R. L. Martin, D. J. Fox, T. Keith, M. A. Al-Laham, C. Y. Peng, A. Nanayakkara, M. Challacombe, P. M. W. Gill, B. Johnson, W. Chen, M. W. Wong, C. Gonzalez and J. A. Pople. *Gaussian03, RevisionB.03.* Gaussian Inc.and Pittsburgh, 2003.

[8] *http://www.openmx-square/org/*

[9] *JCPDS-JCDD, pdf-84-1616*

[10] Æleen Frisch, Micahel J. Frisch and Gary W. Trucks, *Gaussian03 User's Reference*, Gaussian Inc. Carnegie, PA 15106 USA, 2003

[11] N. Nunomura, private communication

[12] D. Costa, K. Sharkas, M. Islam and P. Marcus, *Surface Sci.*, 603 (2009) 2484

[13] M. A. Henderson and S. A. Chambers, *Surface Sci.*, 449 (2000) 135

[14] J. P. Joly, F. Gaillard, E. Peillex and M. Romand, *Vacuum*, 59 (2000) 854

[15] S. Glasstone, K. J. Laidler and H. Eyring, *The Theory of Rate Processes*, McGraw-Hill Book Company, New York and London, 1941

[16] R. J. Madix, G. Ertl and K. Christmann, *Chem. Phys. Letters*, 62 (1979) 38

[17] G. S. Rushbook, *Introduction to Statistical Mechanics*, Clarendon Press, London, 1951